Leading- and Trailing-Edge Flaps on Supersonic Delta Wings

Gloria Hernandez* and Richard M. Wood*
NASA Langley Research Center, Hampton, Virginia
and
Robert E. Collins†
Planning Research Corporation, Hampton, Virginia

An experimental investigation has been conducted to evaluate the effectiveness of leading- and trailing-edge flaps on a flat wing and a cambered wing at supersonic speeds. Experimental testing was conducted at Mach numbers of 1.6, 1.8, 2.0, and 2.16. The study geometry consisted of a clipped delta planform with leading edge swept back 50 deg and trailing edge swept forward 25 deg. Both wings were attached to a generic fuselage and both were configured with identical leading- and trailing-edge flaps. Analysis of the data showed that flap effects are similar for both flat and cambered wings for all aerodynamic parameters. The drag penalty with trailing-edge deflections is lower for the cambered wing compared to the flat wing. The drag penalty on the cambered wing, however, is higher with leading-edge deflections compared to the flat wing. Lift values for the trailing-edge deflections were slightly lower for the cambered wing. Both wings experienced a decrement in lift loss as the Mach number increased. The values for the pitching-moment increments are slightly larger on the flat wing with trailing-edge deflections and smaller on the same wing with leading-edge deflections when compared to the cambered wing.

Nomenclature

C_D = drag coefficient, drag/qS
$C_{D,\min}$ = minimum drag coefficient
C_L = lift coefficient, lift/qS
C_m = pitching-moment coefficient, pitching moment/$qS\bar{c}$
$C_{m,o}$ = zero-lift, pitching-moment coefficient
$\bar{c}$ = mean aerodynamic chord
L/D = lift-to-drag ratio
ℓ = length of root chord, 27.047 in.
M_∞ = freestream Mach number
P_o = tunnel stagnation pressure
R_e = Reynolds number per unit length
S = wing reference area, = 2.25 ft^2
T_o = tunnel stagnation temperature
x = streamwise distance
α = angle of attack, deg
ΔC_D = change in drag coefficient from the value for minimum drag
$\Delta C_D/\Delta C_L^2$ = polar shape factor
ΔC_L = change in lift coefficient from the value for minimum drag
$\partial C_L/\partial\alpha$ = lift-curve slope at $\alpha = 0$
$\partial C_m/\partial C_L$ = longitudinal stability at $\alpha = 0$
δ = flap deflection angle
δ_{LE} = streamwise leading-edge flap deflection (positive when leading edge down), deg
δ_{TE} = streamwise trailing-edge flap deflection (positive when trailing edge down), deg

Presented as Paper 89-0027 at the AIAA 27th Aerospace Sciences Meeting, Reno, NV, Jan. 9-12, 1989; received Feb. 23, 1989; revision received June 10, 1989.

*Aerospace Technologist, Supersonic/Hypersonic Aerodynamics Branch, Applied Aerodynamics Division.
†Mechanical Engineer.

Introduction

VARIABLE camber wings that use leading- and trailing-edge devices are being considered for high-performance aircraft to satisfy the severe aerodynamic requirement of efficient cruise and high-lift across a broad Mach number range. The primary purpose of these leading- and trailing-edge devices is to control the flow on the wing upper surface so that drag is minimized and the pitching moment is controlled at a variety of lift conditions. A typical device is the traditional leading- and trailing-edge flaps which are designed to maintain attached-flow conditions on the wing over a range of lift conditions. Leading- and trailing-edge flaps are typically utilized on production aircraft, but primarily at subsonic and transonic speeds.[1,2] However, previous studies conducted on flat wings indicate that aerodynamic performance benefits can also be obtained by employing leading-edge flaps at supersonic speeds.[3,4] Hence, additional studies are needed to quantify aerodynamic performance benefits associated with leading- and trailing-edge flaps at supersonic speeds for a variety of generic test configurations.

Of particular interest is determining the feasibility of employing leading- and trailing-edge flaps on cambered wings for improved aerodynamic performance at off-design conditions. A wing design program has been established to investigate the effectiveness of leading- and trailing-edge flaps on flat and cambered wings. In support of this program, an experimental investigation of the aerodynamic performance of leading- and trailing-edge flaps on a flat wing and a cambered wing has been conducted in the Unitary Plan Wind Tunnel at low supersonic speeds. Both the flat and cambered wings had the same planform and leading- and trailing-edge flaps arrangements.

Test Description

The tests were conducted in the low Mach number test section of the Unitary Plan Wind Tunnel[5] at Mach numbers of 1.6, 1.8, 2.0, and 2.16 and a Reynolds number of 2×10^6/ft.

An internally mounted, six-component, strain gage balance was used to measure model forces and moments. Based on the manufacturer's stated accuracy for the balance used, the C_D, C_L, and C_m are accurate to within 0.0035, 0.0004, and 0.0006,

respectively. However, repeat points taken for this test indicate that C_D, C_L, and C_m generally repeated within 0.0001, 0.0015, and 0.0001, respectively.

Model angles of attack ranged from -4 to $+20$ deg. Sideslip angles ranged from -8 to $+8$ deg. Leading-edge flaps were tested for deflections of 0–15 deg (positive-leading edge down) in increments of 5 deg. Trailing-edge flaps were tested from -30 to $+10$ deg (positive-trailing edge down) in 10-deg increments.

The model angles of attack were corrected for tunnel-flow angularity and for sting and balance deflection due to aerodynamic loading. Base-cavity pressures were measured and used to correct the force data to a condition of freestream static pressure acting on the base area of the model. The tunnel dew point was held below the minimum value at which condensation effects become significant. Boundary-layer transition strips consisting of a 0.063-in.-wide band of no. 60 grid were located 1.2 in. aft of the fuselage nose and 0.4 in. aft streamwise of the wing leading edge. The method described in Ref. 6 was used to select the grit size and location to provide fully turbulent flow over most of the model at all test conditions.

Model Description

The wings have a clipped delta planform with a leading-edge sweep of 50 deg and trailing-edge sweep of 25 deg (see Fig. 1). Both the cambered and flat wings were configured with leading- and trailing-edge flaps of the same planform. The wings were mounted on a generic fuselage that did not have inlets, canopy, or vertical tail. Using linear-theory methodology,[7] the cambered wing was derived for optimal performance for efficient supersonic cruise with a minimum trim-drag requirement. The cambered wing was designed to meet a broad spectrum of performance goals that included sustained transonic and supersonic maneuver performance, sustained supersonic cruise performance, and acceleration requirements. The multipoint design criteria for the cambered wing was achieved by designing a series of wing-camber surfaces for different lift and Mach number conditions and then evaluating the designs over the flight envelope. In order to meet these performance goals, a wing camber based on a lift coefficient of 0.30 and Mach number of 1.8 was selected as optimum. It should be noted that the optimum is based on an overall mission performance criterion and not aerodynamic performance at specific flight conditions.

Experimental Results

As indicated earlier, the purpose of this study was to evaluate effectiveness of leading- and trailing-edge flaps on flat and cambered wings. The longitudinal aerodynamics of the basic flat and cambered wings with no flap deflections will be discussed first in order to establish the aerodynamics of the basic wings.

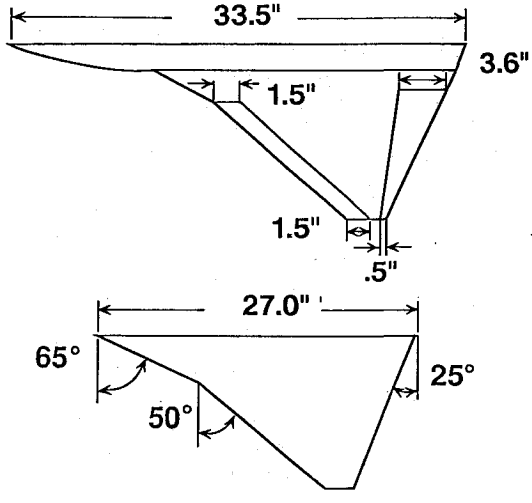

Fig. 1 Sketch of wing geometry

Basic Flat and Cambered Wings Aerodynamic Characteristics—No Flaps

Figures 2 and 3 show the longitudinal aerodynamic characteristics for the basic flat and cambered wings with no leading- and trailing-edge flap deflections at Mach = 1.6 and 2.16, respectively. At Mach = 1.6, the cambered wing has higher drag than the flat wing for lift coefficients below 0.2 (see Fig. 2). At $C_L = 0.2$, a crossover in the drag occurs beyond which the cambered wing has lower drag for all further increases in lift coefficients. The reduced drag value for the cambered wing is a result of a shift in the drag polar as well as a change in the wing polar shape characteristics. This will be discussed for Fig. 4. The L/D max for the cambered wing occurs at $C_L = 0.25$, and the performance of the cambered wing exceeds that for the flat wing for the higher lift conditions. A review of the pitching moment and lift data shows that there is an increase in the zero-lift pitching moment and, for a given angle of attack, there is a decrease in the lift due to wing camber. The data for both wings also show that the variation in C_L and C_m remains linear throughout the test angle-of-attack range.

At the higher Mach number of 2.16 (see Fig. 3), the improved aerodynamic performance due to camber is not realized until about $C_L = 0.25$ at which point there is a slight improvement compared to the flat wing. As observed in the data at Mach 1.6 on Fig. 2, camber continues to provide a positive $C_{m,o}$ shift and a negative shift in the lift coefficient. The data on Figs. 2 and 3 show that at both extremes of the test Mach number range, the cambered wing has improved aerodynamic performance compared to the flat wing. In addition, if

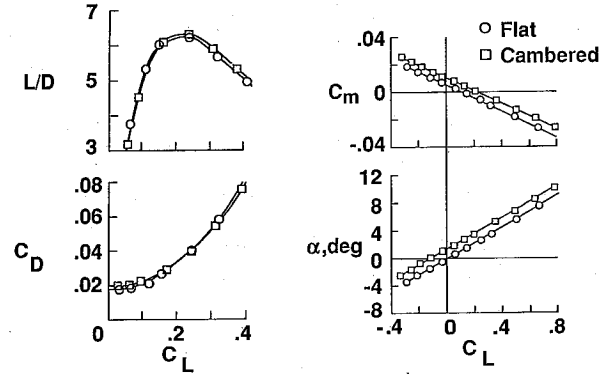

Fig. 2 Longitudinal aerodynamic characteristics $M_\infty = 1.6$, $\delta_{LE} = 0$, $\delta_{TE} = 0$

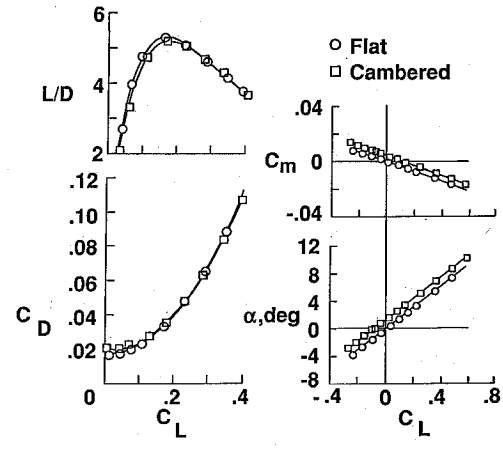

Fig. 3 Longitudinal aerodynamic characteristics $M_\infty = 2.16$, $\delta_{LE} = 0$, $\delta_{TE} = 0$

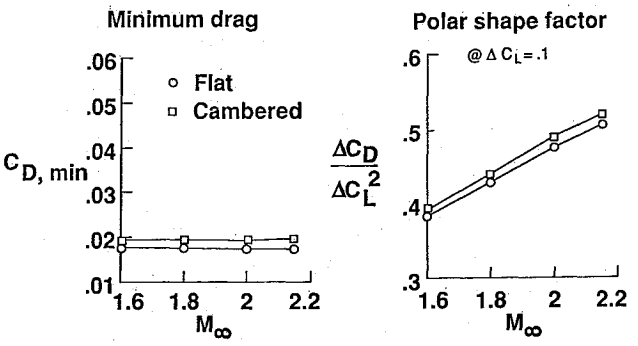

Fig. 4 Drag characteristics on wing $\delta_{LE} = 0$, $\delta_{TE} = 0$

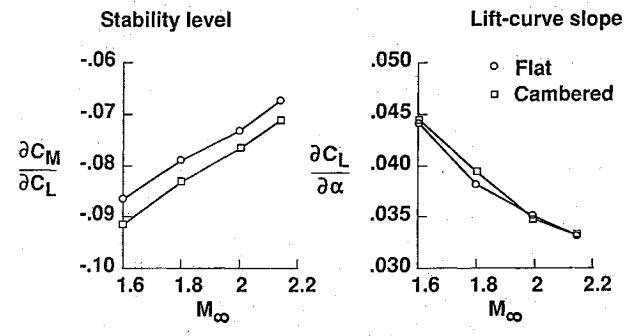

Fig. 5 Stability level and lift-curve slope for flat and cambered wings

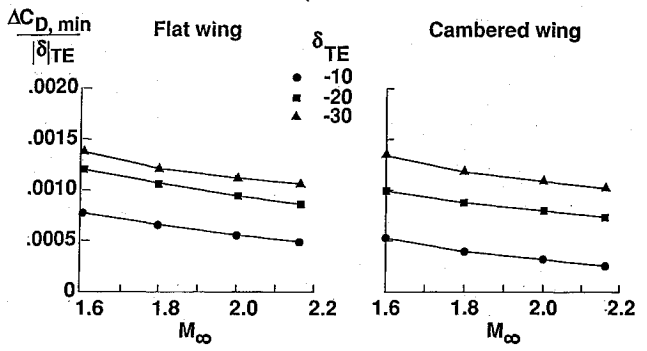

Fig. 6 Effects of trailing-edge flap deflection on minimum drag, $\delta_{LE} = 0$

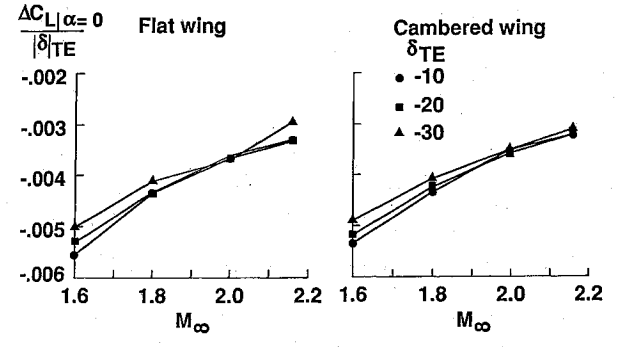

Fig. 7 Effects of trailing-edge flap deflection on lift, $\delta_{LE} = 0$

both wings have the same flap effectiveness, the positive shift in the pitching moment for the cambered wing will significantly improve trimmed lift conditions by requiring a smaller trailing-edge flap deflection for trim compared to the flat wing.

To evaluate further the longitudinal aerodynamics of the basic flat and cambered wings, the aerodynamic characteristics are presented as a function of Mach number in Figs. 4 and 5. Figure 4 shows a comparison of the minimum drag ($C_{D,\min}$) and polar shape factor ($\Delta C_D/\Delta C_L^2$) over the range of Mach numbers tested for the flat and cambered wings. The flat wing data show lower minimum drag, compared to the cambered wing, over the Mach range. The $C_{D,\min}$ data also show that both the cambered wing and flat wing have nearly constant minimum drag over the Mach range. The variation in the polar shape factor with Mach number for the two wings is also presented in Fig. 4. As previously observed, the flat wing shows better performance, lower minimum drag values, compared to the cambered wing for the complete range of Mach numbers. Note that the polar shape factor is an assessment of the drag due to lift referenced from its minimum drag value to its drag values at a ΔC_L of 0.1.

Presented in Fig. 5 are the longitudinal stability level ($\partial C_m/\partial C_L$) and lift-curve slope ($\partial C_L/\partial\alpha$) of the flat and cambered wings for all Mach numbers tested. The data show that both wings exhibit a small increase in stability at the lower Mach numbers, and the cambered wing is slightly more stable than the flat wing over the Mach range. This change in stability is probably due to a change in wing-body interference effects. Figure 5 also shows the rate of change of lift coefficient with angle of attack for the complete Mach number range. The data show that both wings have similar characteristics over the Mach number range tested.

Flap Effectiveness

As mentioned previously, the purpose of this study was to evaluate the effectiveness of leading- and trailing-edge flaps on flat and cambered wings. And as shown in Figs. 2–5, the aerodynamics of the baseline flat and cambered wings are quite similar with the primary differences being in the minimum drag and pitching moment at zero lift. Based upon these differences, it was decided that the figures of merit for assessing leading- and trailing-edge flap effectiveness would be the increments in drag, lift, and pitching moment per degree of flap deflection. This method of presentation should allow for a direct comparison between the flat and cambered wings. All of the flap effectiveness data will be presented as the change in the particular aerodynamic coefficient from the undeflected case divided by the absolute value of the deflection angle. These data will be presented for the trailing-edge flap followed by the data for the leading-edge flap.

Figures 6–8 show the trailing-edge flap effectiveness for the flat and cambered wings over the Mach number range at 0 deg angle of attack. Figure 6 presents the effects on drag and shows that the drag penalty decreases slightly with increasing Mach number. The data of Fig. 6 also show that the drag increment varies nonlinearly with flap deflection. The data for both the flat and cambered wings show that there is a nonlinear increasing drag increment with increasing deflection. The cambered wing data show a lower drag penalty for both the -10-deg and -20-deg deflections when compared to the flat wing. For a -30-deg trailing-edge deflection, both wings have comparable drag values.

The effects of trailing-edge deflection on lift is presented in Fig. 7 for both wings over the Mach number range. The flat and cambered wing data of Fig. 7 show a reduction in lift loss with increasing Mach number. At the lower Mach numbers, there is a slightly larger effect of trailing-edge deflection than at the higher Mach numbers.

Figure 8 shows the change in the zero-lift pitching moment for the trailing-edge flap deflection for the flat and cambered wings. The data for both wings show that the increment due to flap deflection becomes smaller with increasing Mach number. The effectiveness of the flaps decreases with increasing (more negative) flap deflection angle; i.e., the -10-deg-trailing-edge flap deflection has a higher effectiveness per degree than either

the −20-deg-deflection or the −30-deg-deflection for both wings. This difference in effectiveness for the various flap deflections is not as significant for the cambered wing as it is for the flat wing.

Figures 9–11 show the effectiveness for the leading-edge flap deflection over the Mach number range at 0-deg angle of attack. The leading-edge flap effectiveness values are in general an order of magnitude smaller than those for the trailing-edge flaps. The reasons for the reduced impact of the leading-edge flaps compared to the trailing-edge flaps are that the leading-edge flaps are on a swept edge, and their planform area is less and is distributed fore and aft about the moment center.

Figure 9 shows the effects on drag for the leading-edge deflection. No significant variation in the drag increment over the Mach number range is observed; however, the penalty in drag is considerably higher as the leading-edge deflection increases. The drag penalty for the leading-edge flap deflection is considerably higher for the cambered wing than for the flat wing at each deflection. This increased penalty is undoubtedly due to flow separation on the cambered wing.

The variation of the effect on lift with Mach number is shown in Fig. 10. The lift for the cambered wing generally increases with increasing Mach number for all flap deflections, whereas the lift for the flat wing is nearly constant with an increasing Mach number.

The effect of leading-edge flap deflection on the change in zero-lift pitching moment value for the flat and cambered wing is shown in Fig. 11. These data show a trend with an increasing Mach number similar to that observed with the trailing-edge flap (Fig. 8). Note that there is a sign change in the pitching-moment parameter between Figs. 8 and 11. In both Figs. 8 and 11, the largest pitching-moment increment occurs at a Mach number of 1.6, and the increment is reduced with the increasing Mach number. Increasing flap deflection angle results in a nonlinear increase in effectiveness.

The data presented in Figs. 6–11 show that wing camber significantly alters flap effectiveness. In particular, for both trailing-edge and leading-edge flap deflections, the drag increment was higher and lift and pitching moment were lower for the cambered wing compared to the flat wing. To evaluate these effects further, selected flow visualization data will be presented. Flow visualization data were also obtained to provide insight into the cause of the nonlinear aerodynamics.

Flow Visualization

Tufts and oil-flow data were used to examine the flow characteristics on the wing surface, and vapor-screen data were used to examine the flowfield above the wing. On the wing surface, the flow direction is determined by the alignment of the tufts or the streaking of the oil. Both the tufts and the oil flows are affected by the velocity direction near the surface and, in addition, the oil flow pattern is also influenced by the local surface pressures. All of the tuft photographs presented were taken of the upper surface of the wing panel. The vapor-screen data were used to obtain information on the shape and location of vortices and shocks in the flowfield above the wing.

Figure 12 shows tufts on the flat wing at Mach of 1.6 with no leading- or trailing-edge deflections at four different angles of attack of 0, 4, 8, and 12 deg. At 0-deg angle of attack, attached flow over the wing is observed. As the angle of attack increases to 4 deg, the flow accelerates about the leading edge as indicated by the slight inboard alignment of the tufts along the leading edge. A crossflow shock occurs on the wing upper surface as the angle of attack is increased to 8 deg as indicated by the streamwise alignment of tufts on the inboard portion of the wing. At 12-deg angle of attack, a crossflow shock-induced vortex has formed which is indicated by the outboard alignment of the tufts diagonally across the wing.

Presented in Fig. 13 are vapor-screen photographs for the flat wing without a leading- or trailing-edge deflection at angles of attack of 4, 8, and 12 deg. The photographs were taken of the upper surface of the left wing panel at wing locations from the root chord of 30 and 90% at a Mach number of 1.6 with the camera behind the model and looking upstream. The top three photographs are at $x/\ell = 0.30$. The crossflow shock can be seen at an angle of attack of 4 deg (slightly darkened

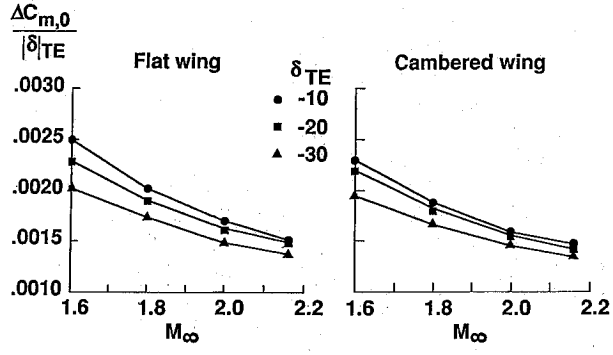

Fig. 8 Effects of trailing-edge flap deflection on zero-lift pitching moment, $\delta_{LE} = 0$

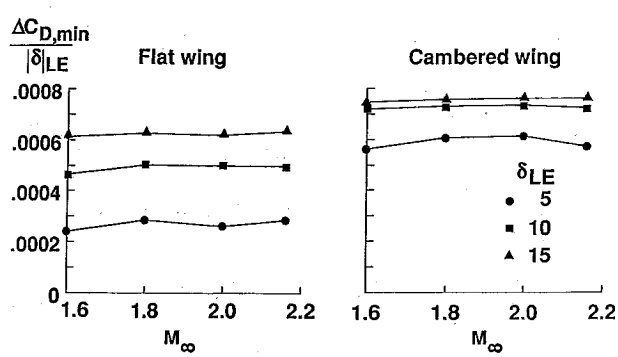

Fig. 9 Effects of leading-edge flap deflection on minimum drag, $\delta_{TE} = 0$

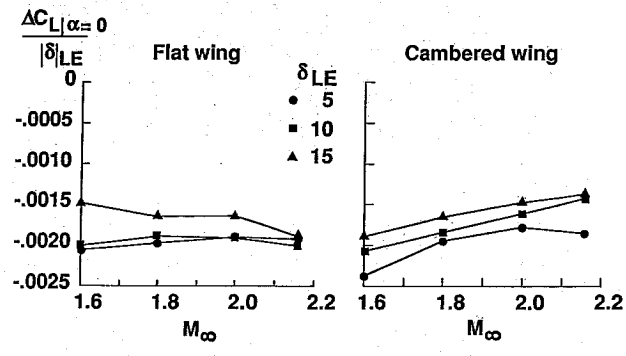

Fig. 10 Effects of leading-edge flap deflection on lift, $\delta_{TE} = 0$

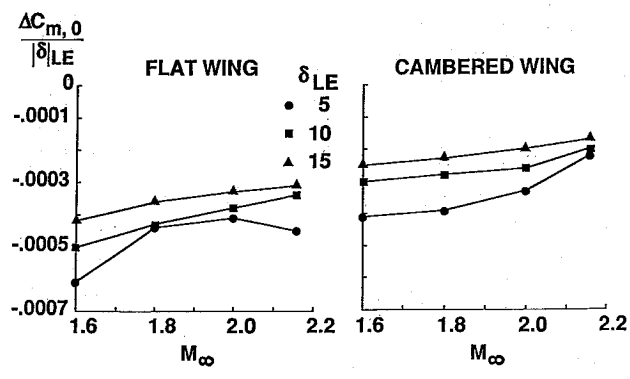

Fig. 11 Effects of leading-edge flap deflection on zero-lift pitching moment, $\delta_{TE} = 0$

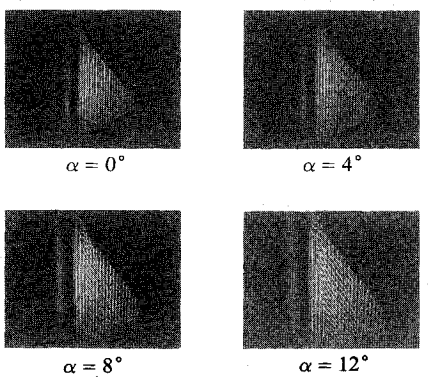

Fig. 12 Tufts on flat wing $\delta_{LE} = 0$, $\delta_{TE} = 0$, $M_\infty = 1.6$

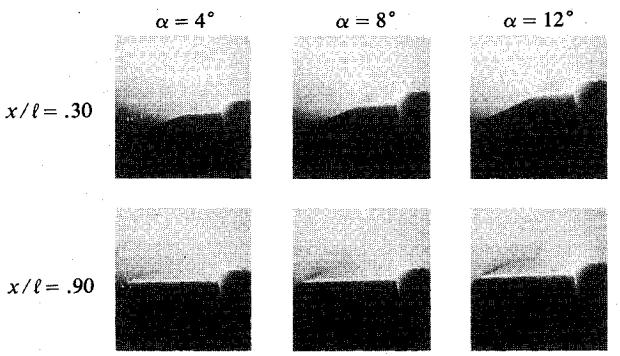

Fig. 13 Vapor screens on flat wing $\delta_{LE} = 0$, $\delta_{TE} = 0$, $M_\infty = 1.6$

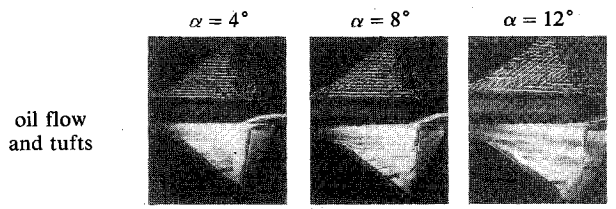

Fig. 14 Flow visualization on flat wing $\delta_{LE} = 0$, $\delta_{TE} = -30$, $M_\infty = 1.6$

region over the wing leading edge). At an angle of attack of 12 deg, the shock increases in strength and a small shock-induced vortex is observed. This vortex can be seen more clearly in the bottom photographs of Fig. 13 at $x/\ell = 0.90$.

Presented in Fig. 14 are oil-flow and tuft photographs of the flat wing with −30-deg trailing-edge flap deflection at $M = 1.6$ and angles of attack of 4, 8, and 12 deg. A review of the 4-deg angle-of-attack oil-flow photographs shows a large detached shock in front of the trailing-edge flap. Forward of the shock, the flow is attached and well behaved. The excellent flow quality on the wing forward of the shock is also evident in the tuft pattern. Behind this shock, the flow would be at a much lower energy state on the upper surface. On the lower surface, the boundary-layer flow would probably separate as it expands about the hinge line. The combination of lower-surface separation and upper-surface shock would result in a reduced flap load and thus a reduced drag increment.

As the angle of attack is increased, the shock in front of the flap moves aft (closer to the flap hinge line), and both the tuft and oil-flow photographs show that the flow over the forward part of the wing is becoming very complex. There appears to be an increase in both the strength of the crossflow shock and the size of the vortex induced by the crossflow shock. The shock in front of the flap is also indicated in the vapor-screen photograph of 4, 8 and 12 deg angle of attack by the horizontal line above the wing. As the angle of attack is increased, the shock moves closer to the wing and, at 12 deg, a crossflow shock is observed near the wing tip.

Concluding Remarks

An experimental investigation has been conducted at supersonic speeds to evaluate the effectiveness of leading- and trailing-edge flaps on a flat and cambered wing. The study geometry consisted of 50-deg swept delta wing with a 25-deg forward swept trailing edge. The cambered wing was designed for a lift coefficient of 0.3 at a Mach number of 1.8. Both wings were attached to a generic fuselage, and both were configured with identical leading- and trailing-edge flaps. Experimental testing was conducted in the low Mach number test section of the Unitary Plan Wind Tunnel at Mach numbers of 1.6, 1.8, 2.0, and 2.16.

Results from the experimental test showed that highly complex and three-dimensional flow can occur over a wing with leading- and/or trailing-edge flaps deflected. Analysis of the data also showed that flap effectiveness varies between a cambered and flat wing of identical planform and flap geometry. Mach number effects are similar for both flat and cambered wings for all aerodynamic parameters.

Drag, lift, and pitching moment were compared for the flat and the cambered wing. There is a 30% decrease in drag penalty per degree of flap deflection for the cambered wing compared to the flat wing data for the −10-deg trailing-edge deflection. The decrease in drag penalty is not as large for the −20-deg deflection with a 17% reduction, and there are no noticeable differences at the −30-deg deflection. The flat wing experiences smaller drag penalties than the cambered wing when leading-edge flaps are deflected—again, with higher drag penalties for the larger flap deflections.

Changes in the flap deflections had little effect on the zero-lift pitching moment. Values for the trailing-edge deflections were slightly lower for the cambered wing. Both wings experienced a decrement in lift loss as the Mach number increased.

The pitching-moment increment per degree of flap deflection is larger at the smaller Mach numbers for both the trailing- and leading-edge flap deflections for both the flat and the cambered wing. The values for the pitching-moment increments are slightly larger on the flat wing with trailing-edge deflections and smaller on the flat wing with leading-edge deflections.

References

[1]Gould, D. K., "Final Report, Variable Camber Wing—Phase I," Research and Engineering Div., Boeing Aerospace Co., D180-17606-1, Oct. 1, 1973.

[2]DeCamp, R. W. and Hardy, R., "Mission Adaptive Wing Advanced Research Concepts," AIAA Paper 84-2088, Aug. 1984.

[3]Wood, R. M. and Covell, P. F., "Experimental and Theoretical Study of the Longitudinal Aerodynamic Characteristics of Delta and Double-Delta Wings at Mach Numbers of 1.60, 1.90, and 2.16," NASA TP-2433, 1985.

[4]Covell, P. F., Wood, R. M., and Miller, D. S., "Investigation of Leading-Edge Flap Performance on Delta and Double-Delta Wings at Supersonic Speeds," NASA TP-2656, 1987.

[5]Jackson, C. M., Jr., Corlett, W. A., and Monta, W. J., "Description and Calibration of the Langley Unitary Plan Wind Tunnel," NASA TP-1905, 1981.

[6]Braslow, A. L., Hicks, R. M., and Harris, R. V., Jr., "Use of Grit-Type Boundary-Layer-Transition Trips on Wind-Tunnel Models," NASA TN D-3579, 1966.

[7]Middleton, W. D., Lundry, J. L., and Coleman, R. G., "A System for Aerodynamic Design and Analysis of Supersonic Aircraft, Part 2—User's Manual," NASA CR-3352, 1980.